García-Fernández, A.; Lozano-Torres, B.; Blandez, JF.; Monreal-Trigo, J.; Soto Camino, J.; Collazos-Castro, JE.; Alcañiz Fillol, M.... (2020). Electro-responsive films containing voltage responsive gated mesoporous silica nanoparticles grafted onto PEDOT-based conducting polymer. Journal of Controlled Release. 323:421-430. https://doi.org/10.1016/j.jconrel.2020.04.048

Electro-responsive films containing voltage responsive gated mesoporous silica nanoparticles grafted onto PEDOT-based conducting polymer

Alba García-Fernández,[a,b,c,d,†] Beatriz Lozano-Torres,[a,b,c,d,†] Juan F. Blandez,[a,d] Javier Monreal-Trigo,[a] Juan Soto,[a] Jorge E. Collazos-Castro,[f,*] Miguel Alcañiz,[a] María D. Marcos,[a,b,c,d] Félix Sancenón,[a,b,c,d,*] and Ramón Martínez-Máñez[a,b,c,d,*]

[a] Instituto Interuniversitario de Investigación de Reconocimiento Molecular y Desarrollo Tecnológico (IDM). Universitat Politècnica de Valencia, Universitat de València, Camino de Vera s/n, 46022 Valencia, Spain.

[b] Unidad Mixta UPV-CIPF de Investigación en Mecanismos de Enfermedades y Nanomedicina, Valencia, Universitat Politècnica de València, Centro de Investigación Príncipe Felipe, València, Spain.

[c] CIBER de Bioingeniería, Biomateriales y Nanomedicina (CIBER-BBN).

[d] Unidad Mixta de Investigación en Nanomedicina y Sensores. Universitat Politècnica de València, IIS La Fe, Valencia, Spain.

[e] Neural Repair and Biomaterials Laboratory, Hospital Nacional de Parapléjicos (SESCAM), Finca la Peraleda s/n, 45071 Toledo, Spain.

† Both authors contributed equally to this work

Abstract

The characteristics and electromechanical properties of conductive polymers together to their biocompatibility have boosted their application as a suitable tool in regenerative medicine and tissue engineering. However, conducting polymers as drug release materials are far from being ideal. A possibility to overcome this drawback is to combine conducting polymers with on-command delivery particles with inherent high-loading capacity. In this scenario, we report here the preparation of conduction polymers containing gated mesoporous silica nanoparticles (MSN) loaded with a cargo that is delivered on command by electro-chemical stimuli increasing the potential use of conducting polymers as controlled delivery systems. MSNs are loaded with Rhodamine B (Rh B), anchored to the conductive polymer poly(3,4-ethylenedioxythiophene) (PEDOT) doped with poly[(4-styrenesulfonic acid)-co-(maleic acid)], functionalized with a bipyridinium derivative and pores are capped with heparin (**P3**) by electrostatic interactions. **P3** releases the entrapped cargo after the application of -640 mV voltage *versus* the saturated calomel electrode (SCE). Pore opening in the nanoparticles and dye delivery is ascribed to both (i) the reduction of the grafted bipyridinium derivative and (ii) the polarization of the conducting polymer electrode to negative potentials that induce detachment of positively charged heparin from the surface of the nanoparticles. Biocompatibility and cargo release studies were carried out in HeLa cells cultures.

Keywords

controlled release, electro-responsive, voltage-gated MSNs, conducting polymers, PEDOT

1. Introduction

Research in the area of gated materials for applications in controlled release protocols has boosted in the last few years [1-3]. These hybrid materials are mainly composed by two subunits namely (i) an inorganic porous scaffold in which a cargo is loaded and (ii) capping molecular or supramolecular ensembles grafted onto the external surface of the material that can be opened upon the application of selected external stimuli [4-7]. Depending on the gated ensemble, cargo release can be triggered in these hybrid materials by stimuli such as pH changes, redox reactions, light, temperature, ultrasounds, and the presence of enzymes or (bio)molecules [8-13]. In fact, the possibility to deliver the cargo on-command upon the presence or application of a certain stimulus is an important issue in the design of delivery systems, in contrast with passive delivery, where cargo is released usually by simple diffusion or after a degradation of the carrier [14-16].

Among stimuli studied to induce cargo release in gated materials, the use of redox processes has been widely explored [17-19]. For instance, redox stimuli have been broadly used for the preparation of gated materials with applications in controlled release protocols in cells based in the presence of high intracellular concentrations of reducing agents such as glutathione. Using this and similar approaches, a number of examples of redox-responsive capped nanoparticles have been described [20-23]. In contrast, there are only few examples in which cargo delivery from mesoporous silica nanoparticles (MSNs) is induced by the application of a voltage. In this area, reported examples involve the use of MSNs functionalized with ferrocene derivatives and capped by an inclusion complex formed between a grafted ferrocene derivative and β-

cyclodextrin (β-CD) [24-27]. However, the use of these ferrocene-based system in biological applications is somehow limited due to the relatively high potential needed (ca. 1-1.5V) to induce ferrocene oxidation and cargo delivery.

From another point of view, conducting polymers are a class of organic materials with electrical properties similar to those of inorganic semiconductors and metals [28]. Moreover, the possibility to assemble these polymers into supramolecular structures has boosted their use in myriads of applications such as organic solar cells [29], printing electronic circuits [30], organic light-emitting diodes [31], etc. One of the most appealing uses of conducting polymers is perhaps their potential application in biomedicine [32,33]. For instance, these polymers have been used, among other applications, as biosensors [34], bioactuators [35], neural interfaces [36-38], drug delivery systems [39,40], tissue engineering scaffolds [41,42], etc. As drug delivery systems, conducting polymers have been loaded with different molecules that are released upon the application of an electric potential. Usually, drug delivery process is based in the change of different redox states of the polymers. These changes results in discharge of the dopant molecules from the materials to the bulk solution [43-45]. However, conducting polymers as drug release materials are far from being ideal and several limitations have prevented their wide use in controlled release applications. For instance, conducting polymers have a limited drug loading capacity, the range of drugs that can be used is restricted due to charge and size requirements and show the inherent release of poorly adsorbed (bio)molecules even without the application of an electric stimulus. Moreover, although it has been reported that drugs delivered from conducting polymers could be suitable for local delivery applications [46,47], the amount of drug

delivered should still be increased for their applications in a majority range of diseases.

A possibility to overcome these drawbacks is to combine conducting polymers with on-command delivery particles with inherent high-loading capacity. The benefits to develop these systems set up the basis of smart materials able to keep applications of conducting polymers (such as monitorization, electrostimulation, etc.) with the additional ability to release the cargo upon the application of a selected stimulus. In this way, the biological applicability of conducting polymers could be enlarged in fields such as neural regeneration and others in which drug delivery can be finely tuned to provide selective control of glial and neuronal cell biology [48].

The high-encapsulation capacity, biocompatibility and the ability of gated MSNs to release different cargos on demand, makes them ideal carriers to be combined with conducting polymers. However, the implementation of MSNs onto conducting polymers is a scarcely studied field and, as far as we know, only one example with polypyrrole has been described [49]. In this example, MSNs were loaded with a nerve growth factor, deposited onto polypyrrole and the effect of drug diffusion in combination with polymer electrical stimulation was studied in PC12 cells. MSNs were used only as carrier to improve the host capacity of the polymer and protection of the molecule, but are not stimuli responsive. Bearing in mind the concepts described above, herein, we present the design, preparation and characterization of a composite based on the combination of poly(3,4-ethylenedioxythiophene) doped with poly[(4-styrenesulfonic acid)-*co*-(maleic acid)] (PEDOT:PSS-*co*-MA) conductive polymer and MSNs that are triggered by voltage stimuli (composite **P3**). MSNs

are loaded with rhodamine B (Rh B, as model molecule) and anchored to the PEDOT:PSS-*co*-MA conducting polymer. The external surface of the nanoparticles is functionalized with a bipyridinium positively charged derivative and the pores capped upon addition of the negatively charged polysaccharide heparin. **P3** is able to release Rh B by the application of a voltage. Pore opening and Rh B release in the nanocomposite is ascribed to both (i) the reduction of the bipyridinium derivative grafted onto the external surface of the nanoparticles and (ii) the polarization of the conducting polymer electrode to negative potentials. These factors induces the detachment of negatively charged heparin from the surface of the nanoparticles allowing cargo delivery. Besides, **P3** films are used for the controlled release of Rh B in cell cultures of HeLa cells in order to corroborate the application of the system and its biocompatibility.

2. Results and discussion.

2.1. Design and characterization of voltage-responsive nanoparticles

The main objective of this paper is to develop a new nanocomposite by the covalent anchoring of redox-triggered gated mesoporous silica nanoparticles (**S3**) onto PEDOT:PSS-*co*-MA conductive polymer. For this purpose, in a first step, **S3** nanoparticles were prepared and the release of an entrapped cargo upon the application of a voltage was studied. In a second step, **S3** was covalently attached onto the conductive polymer yielding nanocomposite **P3**. Application of an external potential induced cargo release from the nanoparticles on **P3**.

The voltage-responsive MSNs **S3** are depicted in Scheme 1. Surface of rhodamine B loaded MSNs was functionalized with a positively charged *N*,*N*'-dimethyl-4,4'-bipyridinium derivative (also known as paraquat or methyl viologen) and capped with the negatively charged polysaccharide heparin via electrostatic interactions. Methyl viologen was selected because its well-known redox properties and easy reduction at relatively low potentials (*vide infra*) [54,55]. Moreover, heparin (a sulfonated polysaccharide) is a biocompatible cap that for instance has been used to improve neuronal growth, cell proliferation and migration [56,57]. The electrostatic interaction between bipyridinium derivate and heparin on the external surface of the nanoparticles is expected to inhibit cargo release. In contrast, reduction of bipyrinium by applying a voltage will induce loss of its positive charge, which would result in a weakening of electrostatic interaction with the negatively charged heparin, the detachment of the polysaccharide from the surface and Rh B release.

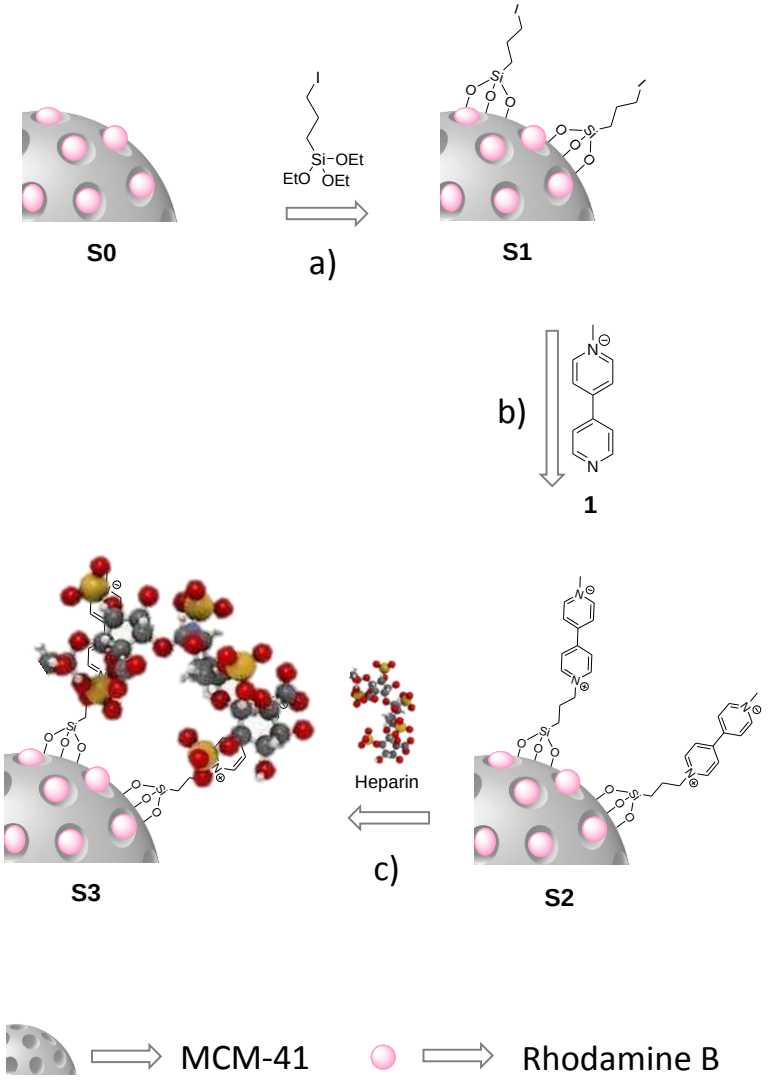

Scheme 1. Schematic representation of the synthesis of voltage-responsive **S3** nanoparticles. MSNs are loaded with Rhodamine B (**S0**) and functionalized with (3-iodopropyl) trimethoxysilane (**S1**). The obtained nanoparticles are reacted with **1** by nucleophilic substitution to yield **S2**. Finally, nanoparticles were suspended in heparin PBS solution, yielding the final heparin-capped solid (**S3**).

MSNs as made and calcined MSNs together with solids, **S1**, **S2** and **S3** were characterized using standard techniques. Contents of Rh B, 3-iodopropyl, bipyridinium dication and heparin for the studied solids were determined by TGA, elemental analysis and ICP-MS (Table 1, Supporting Information and Figure S4). The powder X-ray (PXRD) patterns of calcined MSNs is typical for

mesoporous silica materials with four low-angle peaks characteristic of a hexagonal-ordered pore array indexed as (100), (110), (200) and (210) Bragg reflections. The (100) reflection is still observed in the PXRD pattern of **S1**, **S2** and **S3** (Figure 1, c-e), which evidences that the mesoporous scaffold was maintained in the final nanoparticles. TEM analysis of the nanoparticles showed alternated black and white stripes and a pseudo-hexagonal array of pores, typical of mesoporous systems (Figure 1, right).

Table 1. Amounts (α) of loaded dye and anchored groups in **S1**, **S2**, **S3** and **S4** nanoparticles.

Solid	α_{dye} [mmol g^{-1} SiO_2]	$\alpha_{3\text{-iodopropyl}}$ [mmol g^{-1} SiO_2]	$\alpha_{bipyridinium}$ [mmol g^{-1} SiO_2]	$\alpha_{heparin}$ [g g^{-1} SiO_2]	$\alpha_{3\text{-aminopropyl}}$ [mmol g^{-1} SiO_2]
S1	-	0.24	-	-	-
S2	-	0.24	0.24	-	-
S3	0.24[a]	0.24	0.24	0.03	-
S4	0.25[a]	-	-	-	0.40

[a] Content of Rhodamine B was only determined in the final solids **S3** and **S4**.

From N_2 adsorption–desorption isotherm studies the total specific surface of the calcined starting MSNs was calculated to be 1298.3 m^2 g^{-1}. Besides, the calculated pore diameter and pore volume were 2.36 nm and 0.82 cm^3 g^{-1}, respectively. Similar studies on **S1** revealed a significant decrease in the N_2 volume adsorbed and values of 409.8 m^2 g^{-1} and 0.11 cm^3 g^{-1} were obtained for

the specific surface area and pore volume, respectively (Table S1 and Figure S5).

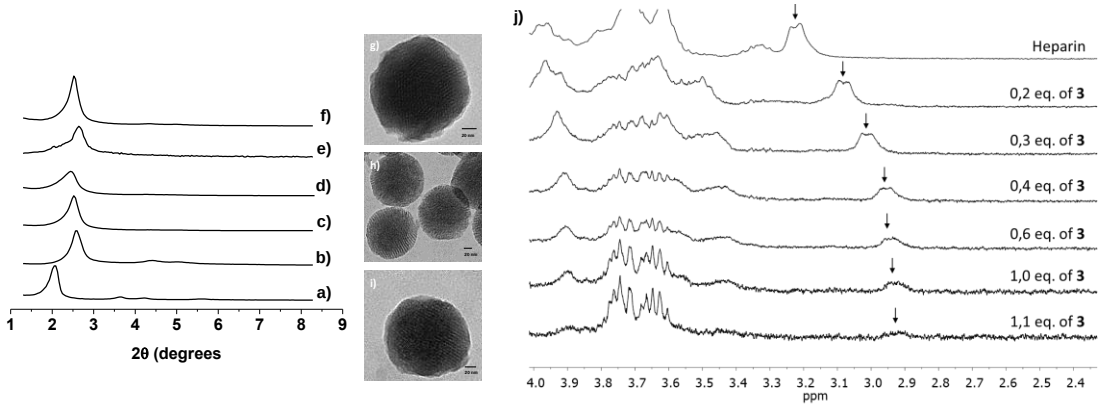

Figure 1. Characterization of the prepared MSNs. Powder X-ray diffraction (PXRD) patterns of solids (a) MSNs as synthesized, (b) calcined MSNs, (c) solid **S1** (d) solid **S2** (e) solid **S3** and (f) solid **S4**. TEM images of (g) calcined MSNs, (h) solid **S3** and (i) solid **S4** showing the typical porosity of the mesoporous matrix. (j) ^{1}H-NMR shifts of heparin protons in the presence of increasing quantities of *N*,*N*'-dimethyl-4,4'-bipyridinium diiodide (compound **3**, mimicking bipyridine-heparin interactions) in D_2O.

Moreover, in order to characterize the heparin-bipyridinium interactions, responsible of the capping mechanism in **S3** and **P3**, ^{1}H-NMR studies were carried out using heparin solutions in D_2O treated with increasing amounts of *N*,*N*'-dimethyl-4,4'-bipyridinium dication (**3**). ^{1}H NMR spectrum of heparin showed the typical signals of polysaccharide protons directly linked to hydroxyl moieties in the 3.6-4.4 ppm range and a broad doublet at ca. 3.31 ascribed to protons in the sugar backbone directly linked to a sulfonamide group (Figure 1j). Addition of increasing quantities of **3** induced moderate upfield shifts of the polysaccharide protons (3.5-4.2 ppm) and a remarkable upfield shift for the proton linked to the sulfonamide unit (from 3.31 to 3.03 ppm). The observed

shifts are ascribed to interactions between heparin and bipirydinium derivative **3**. Based on ^{1}H-NMR titration results, the affinity constant of bipyridine derivative **3** with heparin was calculated to be (5.7 ± 0.69) x 10^{4}.

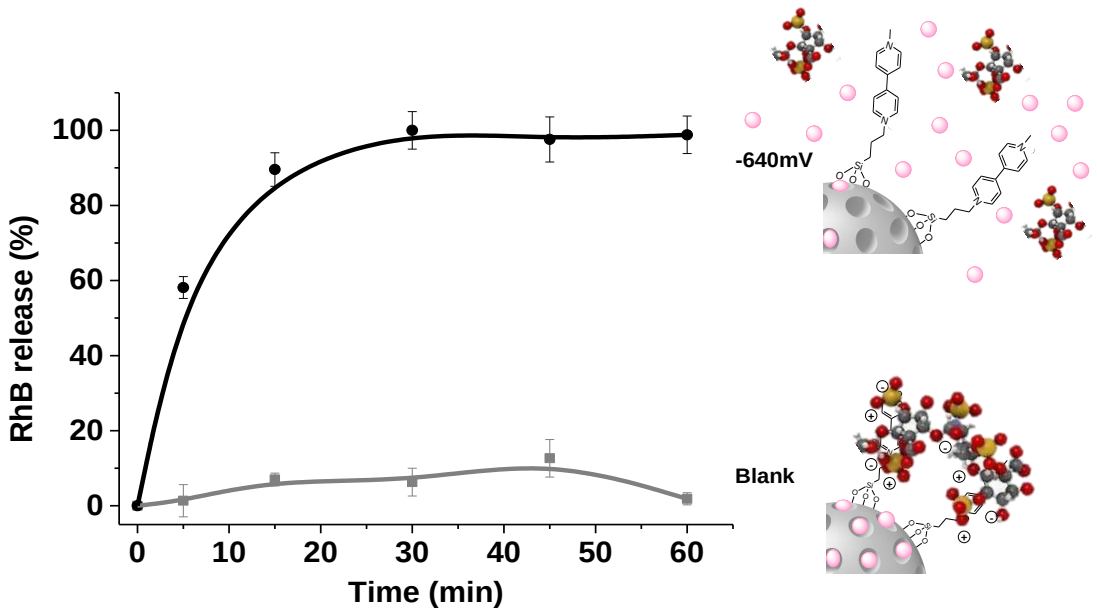

Figure 2. Release profiles of Rh B from **S3** nanoparticles in PBS at pH 7.5 alone and upon the application of a -640 mV vs SCE potential.

For Rh B release experiments from heparin-capped MSNs **S3**, first we carried out studies of the redox properties of methyl viologen (compound **3**) and the carboxylic derivative **2**. Previous reported studies described that the methyl viologen dication displays a one-electron reduction at -615 mV vs. SCE [58]. In our conditions, we found reduction values of -600 mV for **3** and -605 mV vs. SCE for **2**, respectively.

Once electrochemically characterized the methyl viologen derivatives, controlled Rh B delivery experiments from **S3** were carried out in an electrochemical cell by applying an electric potential of -640 mV vs SCE. The

potential of -640 mV vs. SCE was selected considering the electrochemical studies carried out on molecule **3** (*vide ante*). The release profiles from **S3** are shown in Figure 2. In absence of electric potential a low Rh B release was observed (ca. 7% of the maximum Rh B delivered after 60 min), however, when a continuous -640 mV vs. SCE potential was applied a marked dye release was found that reached its maximum after only 30 min. Moreover, similar delivery profiles were observed when PBS suspensions of **S3** were treated with the reducing agent acetaldehyde (Figure S6), which strongly suggests that Rh B delivery was due to the reduction of the grafted bipyridinium. As explained above, reduction of bipyridinium induces a decrease in the positive charge of this molecule, which weakens the electrostatic interaction with the negatively charged heparin, overall resulting in a detachment of the polysaccharide from the surface of the nanoparticles and cargo release. This detachment of heparin from **S3** was assessed in additional experiments. Thus, sulfur content (by ICP-MS) in solution was determined when **S3** nanoparticles were suspended in water in the presence and in the absence of the electrochemical stimuli (both, a voltage of -640 vs. SCE or addition of acetaldehyde). Whereas sulfur content in solution was negligible in the absence of stimuli, an important increase of sulfur (due to heparin) was found upon application of the electrochemical stimuli.

2.2 Design and characterization of voltage-responsive PEDOT:PSS-*co*-MA composites bearing heparin-gated nanoparticles

For the preparation of the bipyridinium-heparin gated nanoparticles we used MSNs (**S0**) and functionalized them with (3-aminopropyl) triethoxysilane in order to obtain **S4**. PEDOT:PSS-*co*-MA polymer was electro-synthesized on

Au-coated surfaces (**P0**). Then, **S4** nanoparticles (loaded with Rh B and functionalized with aminopropyl moieties) were covalently attached onto the PEDOT:PSS-*co*-MA polymer through the formation of amide bonds (**P1**). Once **S4** nanoparticles were assembled onto the polymer, the unbounded surface of the MSNs was functionalised with *N*,*N*'-bypiridinium-1-(carboxymethyl)-1'-methyl diiodide (**2**) yielding **P2** films. The final material (**P3**) was obtained by capping the grafted nanoparticles containing positively charged bipyridinium moieties with heparin by electrostatic interactions. Scheme 2 shows the synthetic procedure used for the preparation of material **P3**.

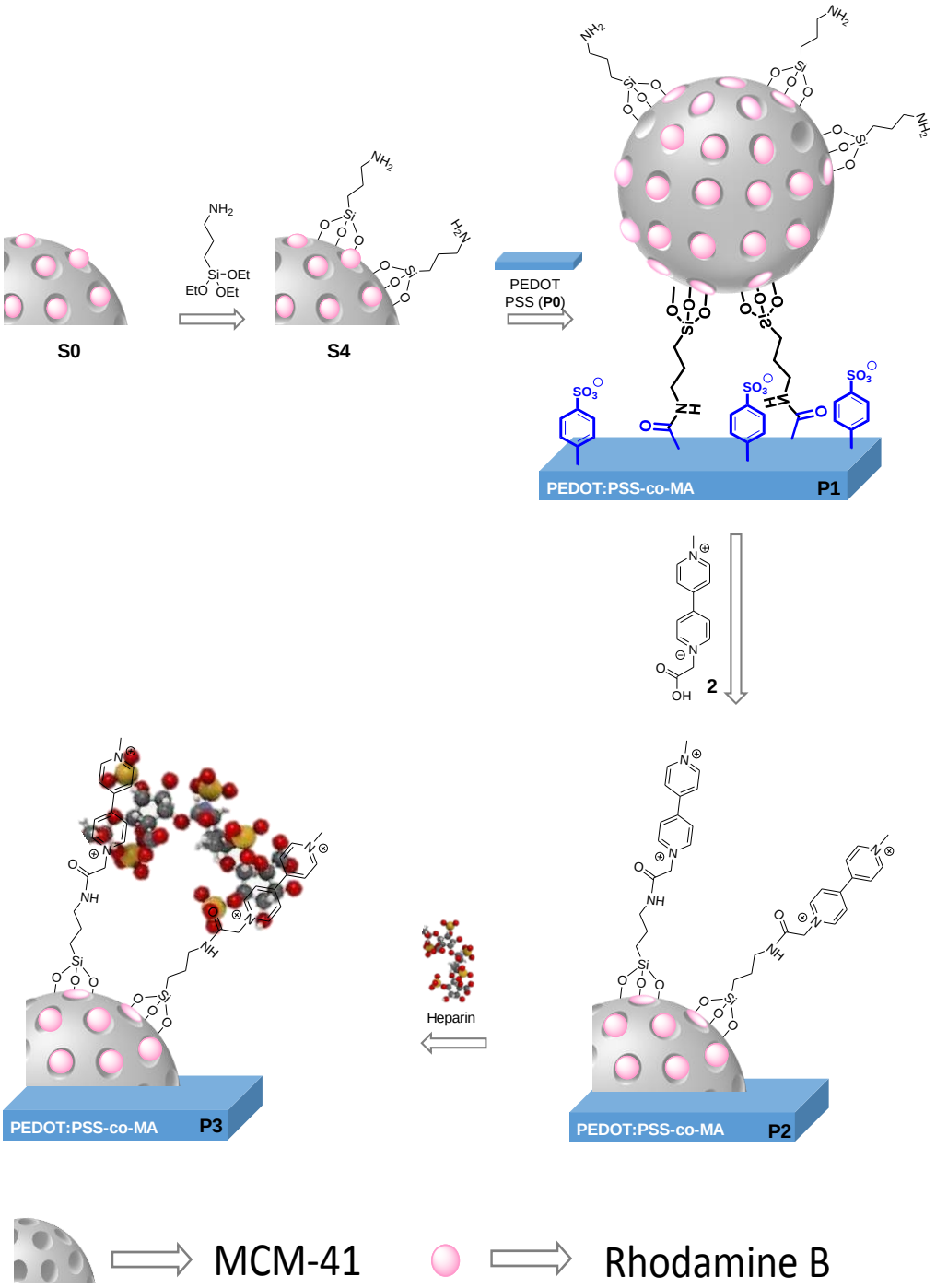

Scheme 2. Synthesis of PEDOT:PSS-*co*-MA films containing heparin-capped MSNs (**P3**). MSNs are loaded with Rh B and functionalized with (3-aminopropyl) trimethoxysilane (**S4**). PEDOT:PSS-*co*-MA material was immersed in an EDC/sulfo-NHS MES buffer solution (pH = 6) in order to activate carboxylic groups. Then, **S4** nanoparticles were added in order to obtain **P1** material. After that, carboxylic acid of 4,4'-bypiridinium-1-(carboxymethyl)-1'-methyl diiodide was activated and then **P1** was immersed into the solution yielding **P2.** Finally, heparin was dissolved in PBS and **P2** was immersed in the solution to obtain **P3** films.

PXRD pattern (Figure 1f) and TEM image (Figure 1i) of **S4** showed the typical features of mesoporous silica nanoparticles. Besides, from N_2 adsorption-desorption measurements, values of specific surface, pore diameter and pore volume of 43.4, 2.36, and 0.07, respectively were determined for **S4** (Table S1). Attachment of the capped MSNs **S4** on the PEDOT:PSS-*co*-MA polymer was assessed by FESEM-FIB (Figure 3). FESEM-FIB images of **P0** (Figure 3a and 3b) showed a surface with no irregularities and a smooth morphology, whereas in images of **P3** (Figure 3d and 3e) spherical MSNs homogeneously distributed over the entire surface were found confirming the attachment of the nanoparticles on the PEDOT:PSS-*co*-MA films. Moreover, confocal microscopy images of **P3** displayed a homogeneously distributed red emission in comparison with **P0** due to the presence of the loaded Rh B in the attached nanoparticles (Figure 3c and 3f). Rh B and heparin content in the final **P3** film amounted to 0.16 mg and 0.65 mg in 1 cm^2 of PEDOT:PSS-*co*-MA scaffold, respectively. In addition, modifications in the surface of PEDOT-MSNs films were confirmed by attenuated total reflectance (ATR) (Figure S7). A typical OH broad band in the 3630 to 3044 cm^{-1} range was found in **P3**. Moreover, peaks at 1614 cm^{-1} due to carboxylates and vibrations at 1209 and 1016 cm^{-1} attributed to symmetric and antisymmetric stretching vibrations of $-SO_3^-$ from heparin were also observed.

P0 and **P2** were also characterized by cyclic voltammetry (Figure 3g and 3h). When **P0** was used as working electrode a reduction peak at -462 mV was observed and attributed to the reduction of the PEDOT film. However, when **P2** was used as working electrode in the same conditions, a shift of the reduction peak from -462 to -557 mV was found, which is tentatively attributed to the

presence of the electroactive methyl viologen derivative in the nanoparticles attached in **P2**.

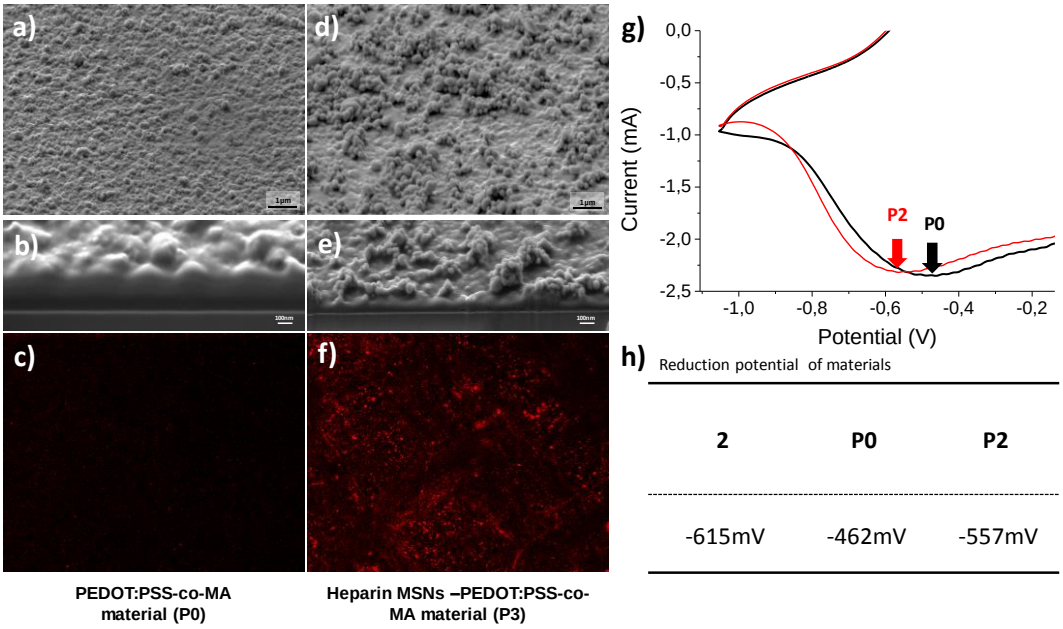

Figure 3. Characterization of PEDOT:PSS-*co*-MA containing heparin-capped MSNs. Left: (a) FESEM-FIB image of **P0** surface, (b) FESEM-FIB image of a cross-section of **P0**, (c) confocal image of **P0**. Right: (d) FESEM-FIB image of **P3** surface, (e) FESEM-FIB image of a cross-section of **P3**, (f) confocal image of **P3**. (g) Cyclic voltammogram of **P0** and **P2** showing the shift of the reduction potential from -462 to -557 mV. h) Reduction potential values for the bipyridinium derivative **2** and the **P0** and **P2** films.

Cargo release from **P3** films was tested in the absence and after the application of an external voltage. The cargo release profiles are shown in Figure 4. In the absence of potential, a low delivery of Rh B was observed (less than 5% after 30 min). In contrast, a significant release of Rh B was found from the **P3** film when a -640 mV vs. SCE potential was applied (ca. 90% of the total dye release after 15 min). Again, as for **S3** nanoparticles (*vide ante*), pore opening and Rh B release is ascribed to the reduction of the grafted

bipyridinium derivative and heparin detachment. Besides, for **P3**, the concomitant reduction of the conducting polymer and its polarization to negative potentials may also help to induce detachment of the negatively charged heparin (due to electrostatic repulsion) from the surface of the nanoparticles. Release studies also revealed that ca. 2 µg of cargo/cm^2 of scaffold were delivered from **P3**, which is ca. 2- to 4-fold larger than typical amounts delivered in reported conducting polymers for drug release applications [46,47]. Similar delivery profiles were found when PBS suspensions of **P3** were treated with the reducing agent acetaldehyde (Figure S8), strongly suggesting that Rh B delivery is redox-controlled. These experiments demonstrate that the modified PEDOT:PSS-*co*-MA conducting polymer **P3** is able to show poor cargo release, yet able to deliver the payload at will upon application of an external voltage.

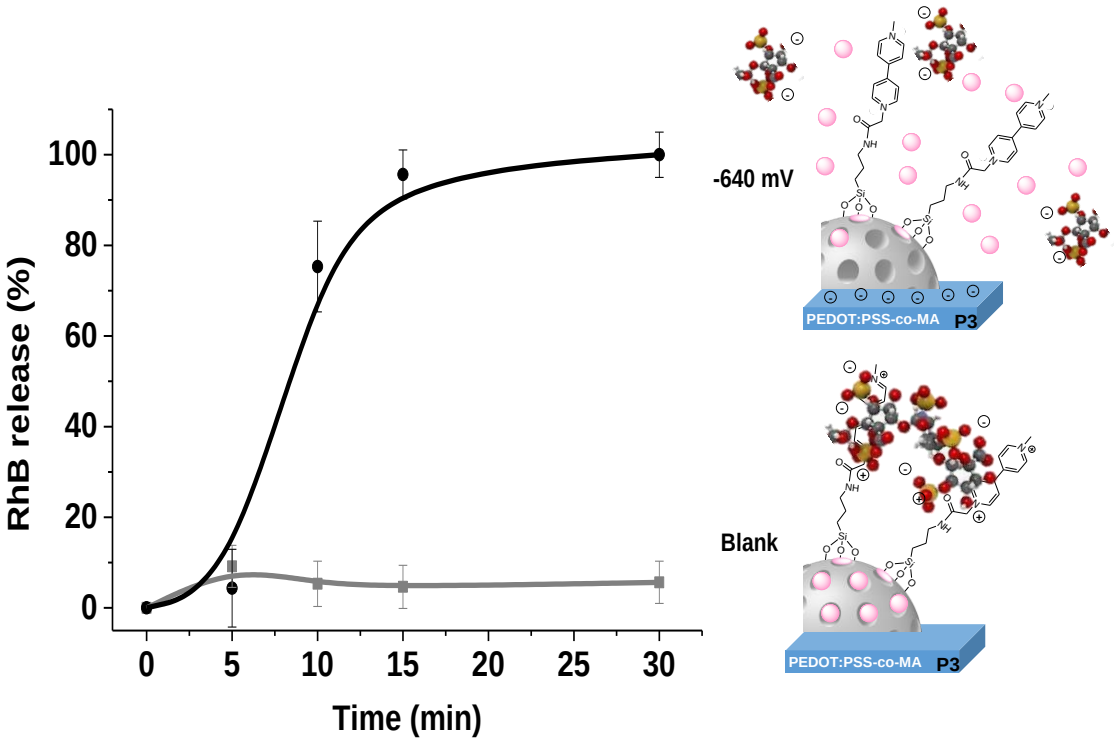

Figure 4. Release profiles of Rh B from **P3** films in PBS at pH 7.5 alone and upon the application of -640 mV vs SCE.

In an attempt to further advance in the potential application of **P3** we tested its biocompatibility and the possibility of using the film to deliver a cargo (i.e. Rh B) by simply applying an external electric voltage to cells in a cell culture medium. To determine biocompatibility, **P0** and **P3** were compared in terms of their ability to support cell growth and proliferation. Moreover, as positive control group, cells were also seeded onto the well-plate surface. Biocompatibility was determined at 48, 72 and 96 h by using the WST-1 assay. Phase contrast microscopy images showed healthy looking adherent cells onto the surface of both, **P0** and **P3** (Figure 5a and 5b) films, this images are in concordance with the viability result obtained after 96 h (Figure 5c), where no significant cell death was observed in the PEDOT-based **P0** and **P3** films.

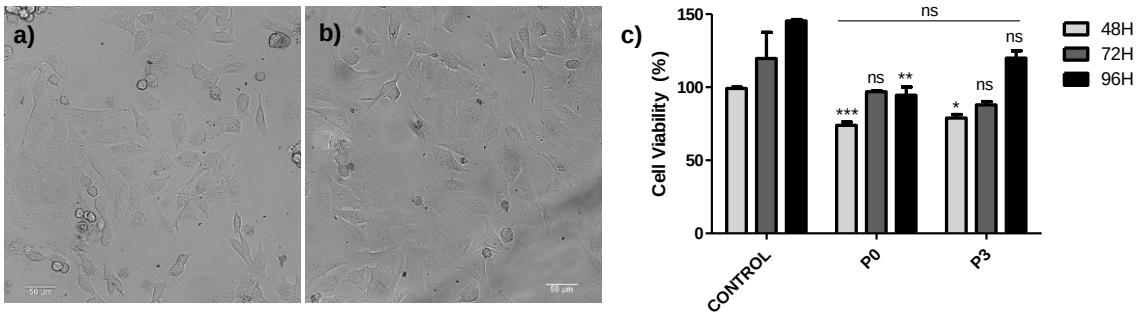

Figure 5. Phase contrast microscope image of HeLa cells on (a) **P0** and (b) **P3** films. (c) Cell viability of HeLa cells seeded onto well-plate surface (control), on **P0** and **P3** after 48, 72 and 96 h. The data represent the mean ± SEM and statistical significance was determined using a one-way ANOVA to compare the different sample groups at predetermined time (* $p < 0.05$, ** $p < 0.025$, *** $p < 0.001$). No significate change can be observe between the different material (**P0** and **P3**), the same result is obtained from **P3** vs control at 96 h.

Moreover, Rh B release studies from the voltage-responsive **P3** composite was tested in the presence of HeLa cells. HeLa cells were seeded over **P3** films that were used as working electrode. A continuous voltage of -600 mV vs. Ag-AgCl was then applied for 15 min and Rh B followed by confocal microscopy. Confocal images of Rh B delivered from **P3** and finally internalized by HeLa cells are shown in Figure 6a. In the absence of potential applied the presence of Rh B inside HeLa cells was negligible after 24 h (t=0). However, after 15 min of voltage application, Rh B emission in HeLa cells was observed with the fluorescence intensity inside cells clearly increasing with time (Figure 6b). Rh B controlled release from **P3** in cell culture was also checked after addition of acetaldehyde as chemical reducing agent (Figure S9) with similar results, strongly suggesting that the Rh B uptake by HeLa cells was ascribed to the voltage-induced Rh B release. These studies demonstrated that the cargo (i.e. Rh B) remained inside the nanoparticles in **P3** even in a complex cell culture medium. Besides, after the delivery experiment FESEM-FIB images of the **P3** films (Figure S10) showed that MSNs remained attached onto the polymeric backbone, indicating that it is the cargo but not the nanoparticles that are delivered from **P3**.

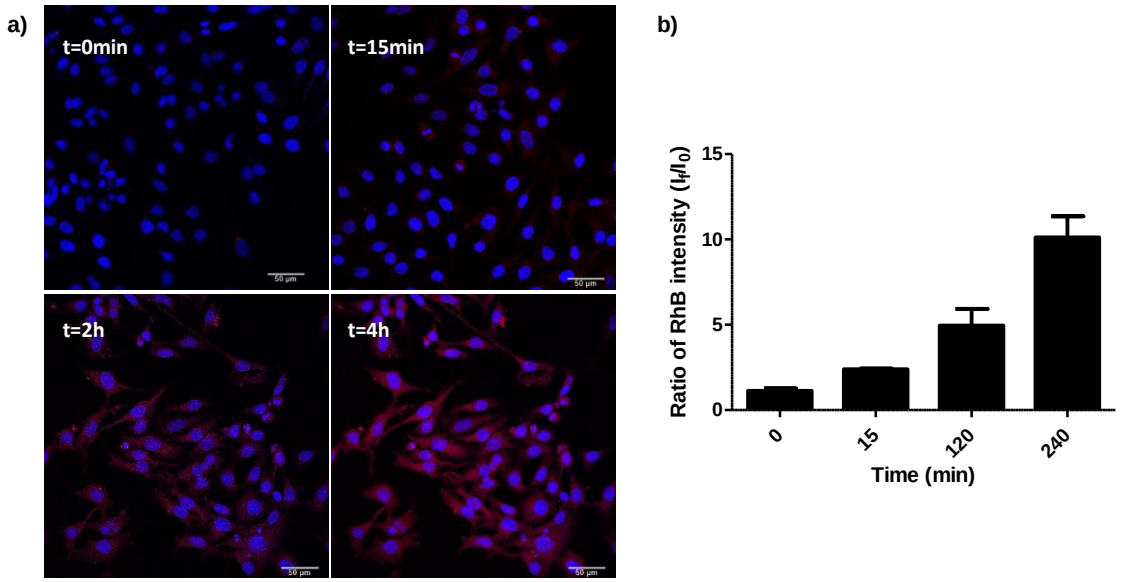

Figure 6. (a) Confocal microscopy images of cellular controlled release studies with **P3**. HeLa cells were examined after 24 h of seeding (t = 0) and upon the application of a continuous -600 mV vs Ag-AgCl potential at t = 15 min, 2 h and 4 h. Rh B associated fluorescence is in red and the cellular nucleus marked with Hoechst 33342 in blue. (b) Ratio of mean fluorescence intensity (I_f/I_0) of Rh B signal in HeLa cells (Image J software analysis) upon the application of a continuous -600 mV vs Ag-AgCl potential at t = 15 min, 2 h and 4 h to film **P3**.

With an aging population and the afflictions of fatal diseases, the development of tools for tissue-engineering and regenerative medicine is of great importance. In this field, the design of conducting polymers with new functionalities is becoming a topic of growing interest. However, their use for drug delivery have some drawbacks such as low loading ability and a poor range of cargos that can be used. To overcome these limitations, we demonstrate that it is possible to combine conducting polymers with gated MSNs able to deliver a cargo upon the application of a voltage. The obtained results prove the use of PEDOT-MSNs films in controlled drug delivery strategies, opening avenues for new applications. For instance, such PEDOT-

MSNs films could be used to both, as neuro–electronic interfaces and lesion-bridging systems and to deliver specific molecules, for uses in nervous system lesions or spinal cord injury. In these scenarios, neuroprotection and regeneration could be promoted by delivering neural growth factors or drugs that enhance the bioactivity of the substrate and enhance cellular growth and axonal elongation [59]. Besides, PEDOT-MSNs films could help in therapy of neurological disorders, such as Parkinson, by stimulating deep brain regions as well as by delivering drugs (dopamine, L-DOPA, etc.) [60].

Some other applications combining electrical stimulation as well as drug release can also be envisioned enhancing the opportunities for tissue repair or for the development of electro-active prostheses for voltage-controlled drug delivery. Thus, conducting polymers have also been used in studies for cardiac muscle regeneration [61]. PEDOT-MSNs could act as electrical nanobridge, by transferring electrical signals between cardiomyocytes and delivering bioactive molecules to promote the recovery of damaged cardiac cells. Otherwise, PEDOT-MSNs looks promising in bone tissue regeneration and wound healing applications. Electrostimulation, combined with drug delivery from MSNs, could be used for promoting faster mineralization or healing by releasing bioactive molecules for mineralization as well as antimicrobials or anti-inflammatory drugs to control bone or skin infection [62]. However, further research is needed to evaluate the potential application of these new materials and studies for specific uses are currently studied by us. Besides, voltage-triggered gated MSNs can be easily adapted to the development of new films attending the easy surface functionalization of MSNs, which opens the possibility to attach the nanoparticles to other conductive polymers. Moreover, gated nanoparticles can also be designed to respond to positive or negative potentials attending the

electrical properties of the selected polymer and their applications. We believe that the results presented herein might inspire the development of new films equipped with gated MSNs for a number of uses in the pharmaceutical and biomedical field.

3. Conclusions

We demonstrate herein that it is possible to combine conducting polymers with gated MSNs able to deliver a cargo upon the application of a voltage. In particular, we prepared MSNs loaded with rhodamine B and capped by an electro-active shell formed by grafted bipyridinium cations and heparin. In the absence of an external voltage heparin-coated MSNs (**S3**) are unable to release the entrapped dye. However, upon the application of a continuous -640 mV vs. SCE potential a marked cargo release is observed. This delivery is ascribed to the reduction of the bipyridinium dication that induced heparin detachment and subsequent pore opening. This mechanism is demonstrated with the addition of acetaldehyde as a chemical reducing agent. We also prepared PEDOT:PSS-*co*-MA conducting polymers in which the capped nanoparticles are covalently attached (**P3** films). The prepared films are able to release the entrapped rhodamine B upon the application of a -640 mV vs. SCE voltage. Cell proliferation studies carried out with HeLa cells show that **P3** films are biocompatible. Besides, the application of a -600mV vs. Ag-AgCl voltage, induced rhodamine B release from the grafted MSNs, which are uptake by HeLa cells. To the best of our knowledge, **P3** is the first example of a PEDOT-based conducting polymer equipped with gated MSNs. **P3** shows a remarkable cargo delivery triggered by the application of an electric potential. Our studies also open the concept to develop conducting polymers combined with capped

MSNs for the on-command delivery of selected cargos using different stimuli for a number of different applications.

4. Experimental section

4.1. Synthesis of MSNs materials and **S3** preparation

Detailed materials and experimental section for (**S3**) nanoparticles obtaining are included in the supporting information. The starting MSNs were synthetized following well established procedures as previously reported [50,51]. Once obtained the starting material, rhodamine B loaded nanoparticles (**S0**), functionalized (**S1** and **S2**) and capped with heparin (**S3**) were prepared.

4.2. Synthesis of *N*-methyl-4,4'-bypiridinium iodide (**1**)

4,4´-bipyiridine (3.0 g, 19.3 mmol) was transferred to a two-necked round bottom flask equipped with a condenser. Anhydrous CH_3CN (120 mL) was added and the system was purged with Argon. Once the solution was at reflux, methyl iodide (1200 µL, 19.3 mmol) was added dropwise and the reaction was maintained at reflux for 12 h. Finally, the solvent was removed under reduced pressure. Product was purified by washing with cold methanol to precipitate the dimethylated compound. Methanol was removed under reduced pressure in order to obtain product (**1**) as an orange solid in 93.9% yield (5.39 g, 18.12 mmol). ^{1}H NMR (400 MHz, D_2O) δ = 8.93 (d, J = 6.7 Hz, 2H), 8.78 (dd, J = 4.6, 1.6 Hz, 2H), 8.40 (d, J = 6.6 Hz, 2H), 7.92 (dd, J = 4.6, 1.4 Hz, 2H), 4.47 (s, 3H) ppm. ^{13}C NMR (400 MHz, D_2O) δ = 153.45, 149.98, 145.62, 142.57, 125.77, 122.48, 47.90 ppm. HRMS-EI m/z: calcd for $C_{11}H_{11}N_2^+$: 171.0917; measured: 171.0914. (Figure S1).

4.3. Synthesis of 3-aminopropyl functionalized MSNs (**S4**)

For the preparation of **S4**, 150 mg of MSNs loaded with rhodamine B **(S0)** were suspended in a saturated solution of Rh B in anhydrous CH_3CN (6 mL). Then, an excess of (3-aminopropyl) trimethoxysilane (175.50 µL, 5 mmol/g solid) was added, and the final mixture was stirred at room temperature for 5.5 h. The resulting pink solid (**S4**) was isolated by centrifugation, washed twice with CH_3CN (5 ml) and dried at 37°C.

4.4. Synthesis of PEDOT:PSS-co-MA (**P0**)

An Autolab PGstat30 galvanostat/potentiostat was used for PEDOT:PSS-*co*-MA electro-polymerization at constant anodic current (100 µA/Cm^2, 96 mC/cm^2 polymerization charge) on gold-coated glass slides. A Pt foil served as counter-electrode and a SCE as reference electrode. The solution for electrodeposition contained 0.16 % (v/v) 3,4-ethylenedioxythiophene (EDOT) and 0.344 % (w/v) PSS-*co*-MA in aqueous potassium phosphate-buffered saline (Milli-Q water with 18.2 MΩ cm^2 containing 9 g NaCl, 0.8 g $Na_2HPO_4 \cdot 2H_2O$ and 0.14 g KH_2PO_4 per liter) [52].

4.5. Synthesis of PEDOT:PSS-*co*-MA films containing MSNs (**P1**)

In a first step, carboxylic groups on the surface of PEDOT:PSS-*co*-MA were activated with a solution of 10 mg/mL of EDC (15 ml) and 10 mg/mL of sulfo-NHS (5 mL) in MES buffer (pH = 6) for 15 min at room temperature. Then 20 mg of **S4** nanoparticles were suspended in 5 ml of PBS buffer (pH = 7.4) and activated PEDOT:PSS-*co*-MA was immersed in the suspension. The reaction was stirred overnight in order to covalently attach MSNs to PEDOT:PSS-*co*-MA, giving **P1**. The final material was washed twice with PBS.

4.6. Synthesis of 4,4'-bypiridinium-1-(carboxymethyl)-1'-methyl diiodide (**2**)

Product **2** was synthesized by nucleophilic substitution reaction between **1** and ethyl bromoacetate. Compound **1** (1.6 g, 5.38 mmol) was transferred to a two-necked round bottom flask equipped with a condenser. Then, anhydrous acetonitrile (18 mL) was added and the system was purged with Argon. Once the reaction was at reflux, ethyl bromoacetate (1500 µl, 12.15 mmol) was added dropwise and the reaction was maintained at reflux for 5 h. Finally, the solid product obtained was filtered off and washed three times with acetonitrile. The intermediate ester was stirred in 200 mL of NaOH 1 M for 10 min and then the solution was acidified until pH = 2 in order to hydrolyze the ester group. The final product was purified by washing with cold methanol. **2** was obtained as an orange solid in 90.2% yield. (1.12 g, 4.85 mmol). ^{1}H NMR (400 MHz, D_2O) δ 9.05-9.02 (m, 4H), 9.02 (d, J = 6.97 Hz, 2H), 8.54 (d, J = 6.73 Hz, 2H), 5.56 (s, 2H), 4.55 (s, 3H). ^{13}C NMR (101 MHz, D_2O) δ 169.34, 150.75, 149.76, 146.70, 146.35, 126.80, 126.75, 62.28, 48.43. HRMS-EI m/z: calculated for $C_{13}H_{15}N_2O_2^{2+}$: 231.1123; measured: 231.1161. (Figure S2).

4.7. Synthesis of PEDOT:PSS-*co*-MA films containing heparin capped-MSNs (**P3**)

Covalent attachment of **2** was carried out through the formation of an amide bond between the carboxylic group in **2** and free amino moieties in MSNs yielding **P2**. For this purpose, the carboxylic group in **2** (73.5 mg, 0.2 mmol) was activated with a solution of 10 mg/mL of EDC (15 ml) and 10 mg/mL of sulfo-NHS (5 ml) in MES buffer (pH = 6) for 15 min at room temperature. Then pH was adjusted to 7.4, **P1** was immersed into the solution and the mixture was

stirred overnight. The final material was washed twice with PBS. Finally, heparin (20 mg, 0.015 mmol) was dissolved in 5 ml of PBS (pH = 7.4) and **P2** was immersed in the solution. After 3 h at room temperature, the final electro-responsive material **P3** was obtained, washed with PBS (pH = 7.4) and dried at room temperature.

4.8. Bypiridinium-heparin interaction studies

In order to assess the interaction between bypiridinium derivatives and heparin, involved in the capping mechanism of **S3** and **P3**, ^{1}H-NMR studies in D_2O were carried out using compound **3** (0.1 M) (Figure S3) and heparin (20 mg/mL). ^{1}H-NMR signals of heparin were monitored after the addition of increasing quantities of **3** (from 0.2 to 1.1 eq.).

4.9. Cargo release studies with **S3** and **P3**

In a first step, for the Rh B release experiments of heparin-capped MSNs **S3**, we carried out studies of redox properties of methyl viologen (compound **3**) and the carboxylic derivative **2** at room temperature with a potentiostat/galvanostat reference PGSTAT100 (Autolab) connected to a PC using an electrochemical cell containing a stainless steel working electrode, a Pt ring counter electrode and a calomel electrode as reference.

Controlled Rh B delivery from **S3** were carried out at room temperature with a potentiostat/galvanostat reference PGSTAT100 (Autolab) connected to a PC using an electrochemical cell with a stainless-steel working electrode (diameter 30 mm, thickness 2 mm), a Pt ring electrode (Crison) as counter electrode and a SCE (Crison) as reference. In a common experiment, 4 mg of solid **S3** were suspended in 12 mL of PBS (10 mM, pH 7.5) in the

electrochemical cell. Release of Rh B from **S3** was studied with and without the application of stimuli (-640 mV vs. SCE potential). At certain fixed times, aliquots were separated, centrifuged to eliminate the solid, and the Rh B released from **S3** was monitored following the emission band at 576 nm (λ_{ex} = 554 nm).

Once performed the delivery studies with **S3,** we move one step forward to monitor the release of Rh B from the heparin-capped nanoparticles grafted onto the PEDOT:PSS-*co*-MA film (**P3**). The experiments were performed with the potentiostat/galvanostat reference PGSTAT100 using an electrochemical cell with **P3** acting as working electrode. The Pt ring electrode (Crison) was used as counter electrode and a SCE (Crison) as reference. **P3** was immersed in 12 mL of PBS (10 mM, pH 7.5). The release of rhodamine B was registered at certain fixed times, in the absence and upon the application of a -640 mV vs. SCE potential. Similar experiments were carried out using (500 µl) acetaldehyde as chemical reducing agent in a similar procedure for **S3** and **P3** respectively. The 100% release was determinate in each experiment by normalizing to the maximum Rh B release achieved (% rhodamine B released = RhB sample/RhB max *100)

4.10. Cell culture conditions

HeLa human cervix adenocarcinoma cells were purchased from the German Resource Centre for Biological Materials (DSMZ) and were growing in DMEM supplemented with 10% FBS. Cells were incubated at 37°C in an atmosphere of 5% carbon dioxide and 95% air and underwent passage twice a week.

4.11. Cell proliferation studies

P0 and **P3** films were first sterilized by exposure to UV light for 30 min and were placed in a 6-well plate. HeLa cells were seeded onto the films at 200,000 cells/mL in DMEM with 10% FBS. Cell viability before starting the experiment was determined by the Trypan Blue method, and the measured viability exceeded 95% in all cases. After 48 h the cell growth was tested by adding the cell proliferation WST-1 reagent for 1 h. After 1 h, 100 µl of the medium containing the WST-1 reagent was placed in a 96-well plate, and the absorbance was measured at 595 nm in a Wallac 1420 workstation. Then, cells were washed with PBS and fresh medium was added. This process was repeated after 72 and 96 h.

4.12. Controlled release of **P3** in cell cultures of HeLa cells

P3 was placed over glass coverslip in a 6 well-plate and then cells were seeded and incubated at 37 °C for 24 h in DMEM. After 24 h of incubation, cells were washed with PBS, and the DNA marker Hoechst 33342 (2 µg/mL) was added to visualize the cells seeded onto **P3** using a confocal microscope (Leica TCS SP8 AOBS). After the evaluation of the cells at 0 min, electrical stimulation was performed using a previously validated homemade electronic equipment designed based on the previously reported FraPlus Mini system [53]. The electrochemical cell included **P3** as working electrode, a Pt (1 mm Ø) electrode as counter electrode and a Ag-AgCl (1 mm Ø) homemade electrode as reference electrode). These electrodes overcame the spatial restriction of being introduced in the 6 well-plate. The applied potential was -600 mV vs. Ag-AgCl (-640 mV vs. SCE). After the application of the potential Rh B released and internalized in cells was monitored by confocal microscopy. Release

experiments were also carried out using acetaldehyde as chemical reducing agent.

ACKNOWLEDGMENTS. Alba García-Fernández, Beatriz Lozano-Torres contributed equally to this work. A. García-Fernández and B. Lozano-Torres are grateful to the “Ministerio de Economía y Competitividad” of the Spanish Government for her PhD fellowships. J. F. Blandez thanks the “Universitat Politècnica de València” for his postdoctoral fellowship (PAID-10-17). The authors thank to the Spanish Government (Projects RTI2018-100910-B-C41 and RTI2018-101599-B-C22 (MCUI/AEI/FEDER, EU)) and the Generalitat Valencia (Project PROMETEO2018-024) for support.

References

[1] E. Aznar, M. Oroval, Ll. Pascual, J. R. Murguía, R. Martínez-Máñez, F. Sancenón, Gated Materials for On-Command Release of Guest Molecules, Chem. Rev. 116 (2016) 561-718.

[2] S. Mura, J. Nicolas, P. Couvreur, Stimuli-Responsive Nanocarriers for Drug Delivery, Nat. Mater. 12 (2013) 991-1003.

[3] A. Llopis-Lorente, B. Lozano-Torres, A. Bernardos, R. Martínez-Máñez, F. Sancenón, Mesoporous Silica Materials for Controlled Delivery Based on Enzymes, J. Mater. Chem. B 5 (2017) 3069-3083.

[4] D. Tarn, C. E. Ashley, M. Xue, E. C. Carnes, J. I. Zink, C. J. Brinker, Mesoporous Silica Nanoparticle Nanocarriers: Biofunctionality and Biocompatibility, Acc. Chem. Res. 46 (2013) 792-801.

[5] C. Mauriello Jimenez, D. Aggad, J. G. Croissant, K. Tresfield, D. Laurencin, D. Berthomieu, N. Cubedo, M. Rossel, S. Alsaiari, D. H. Anjum, R. Sougrat, M. A. Roldan-Gutierrez, S. Richeter, E. Oliviero, L. Raehm, C. Charnay, X. Cattoen, S. Clement, M. Wong Chi Man, M. Maynadier, V. Chaleix, V. Sol, M. Garcia, M. Gary-Bobo, N. M. Khashab, N. Bettache, J.-O. Durand, Porous Porphyrin-Based Organosilica Nanoparticles for NIR Two-Photon Photodynamic Therapy and Gene Delivery in Zebrafish, Adv. Func. Mater. 28 (2018) 1800235.

[6] S. Alberti, G. J. A. A. Soler-Illia, O. Azzaroni, Gated Supramolecular Chemistry in Hybrid Mesoporous Silica Nanoarchitectures: Controlled Delivery and Molecular Transport in Response to Chemical, Physical and Biological Stimuli, Chem. Commun. 51 (2015) 6050-6075.

[7] A. Llopis-Lorente, B. de Luis, A. García-Fernández, S. Jimenez-Falcao, M. Orzáez, F. Sancenón, R. Villalonga, R. Martínez-Máñez, Hybrid Mesoporou Nanocarriers Act by Processing Logic Tasks: Toward the Design of Nanobots Capable of Reading Information from the Environment, ACS Appl. Mater. Interfaces 10 (2018) 26494-26500.

[8] P. Yang, S. Gai, J. Lin, Functionalized Mesoporous Silica Materials for Controlled Drug Delivery, Chem. Soc. Rev. 41 (2012) 3679-3698.

[9] N. Song, Y.-W. Yang, Molecular and Supramolecular Switches on Mesoporous Silica Nanoparticles. Chem. Soc. Rev. 44 (2015) 3474-3504.

[10] M. Oroval, P. Díez, E. Aznar, C. Coll, M. D. Marcos, F. Sancenón, R. Villalonga, R. Martínez-Máñez, Self-Regulated Glucose-Sensitive Neoglycoenzyme-Capped Mesoporous Silica Nanoparticles fon Insulin Delivery, Chem. Eur. J. 23 (2017) 1353-1360.

[11] C. de la Torre, L. Domínguez-Berrocal, J. R. Murguía, M. D. Marcos, R. Martínez-Máñez, J. Bravo, F. Sancenón, ε-Polylysine-Capped Mesoporous

Silica Nanoparticles as Carrier for the *C9h* Peptide to Induce Apoptosis in Cancer Cells, Chem. Eur. J. 24 (2018) 1890-1897.

[12] A. Llopis-Lorente, P. Díez, A. Sánchez, M. D. Marcos, F. Sancenón, P. Martínez-Ruíz, R. Villalonga, R. Martínez-Máñez, Interactive Models of Communication at the Nanoscale Using Nanoparticles that Talk to One Another, Nat. Commun. 8 (2017) 15511.

[13] Ll. Pascual, I. Baroja, E. Aznar, F. Sancenón, M. D. Marcos, J. R. Murguía, P. Amorós, K. Rurack, R. Martínez-Máñez, Oligonucleotide-Capped Mesoporous Silica Nanoparticles as DNA-Responsive Dye Delivery Systems for Genomic DNA Detection, Chem. Commun. 51 (2015) 1414-1416.

[14] C. Argyo, V. Weiss, C. Bräuchle, T. Bein, Multifunctional Mesoporous Silica Nanoparticles as a Universal Platform for Drug Delivery, Chem. Mater. 26 (2014) 435-451.

[15] Z. Li, J. C. Barnes, A. Bosoy, J. F. Stoddart, J. I. Zink, Mesoporous Silica Nanoparticles in Biomedical Applications, Chem. Soc. Rev. 41 (2012) 2590-2605.

[16] P. Kumar, P. Tambe, K. M. Paknikar, V. Gajbhiye, Mesoporous Silica Nanoparticles as Cutting-Edge Theranostics: Advancement from Merely a Carrier to Tailor-Made Smart Delivery Platform, J. Control. Release 287 (2018) 35-57.

[17] C. -Y. Lai, B. G. Trewyn, D. M. Jeftinija, K. Jeftinija, S. Xu, S. Jeftinija, V. S.-Y. Lin, A Mesoporous Silica Nanosphere-Based Carried System with Chemically Removable CdS Nanoparticle Caps for Stimuli-Responsive Controlled Release of Neurotransmitters and Drug Molecules, J. Am. Chem. Soc. 125 (2003) 4451-4459.

[18] R. Liu, X. Zhao, T. Wu, P. Feng, Tunable Redox-Responsive Hybrid Nanogated Ensembles, J. Am. Chem. Soc. 130 (2008) 14418-14419.

[19] H. Qu, L. Yang, J. Yu, T. Dong, M. Rong, J. Zhang, H. Xing, L. Wang, F. Pan, H. Liu, A Redox Responsive Controlled Release System Using Mesoporous Silica Nanoparticles Capped with Au Nanoparticles, RSC Advances 7 (2017) 35704-35710.

[20] C. Giménez, C. de la Torre, M. Gorbe, E. Aznar, F. Sancenón, J. R. Murguía, R. Martínez-Máñez, M. D. Marcos, P. Amorós, Gated Mesoporous Silica Nanoparticles for the Controlled Delivery of Drugs in Cancer Cells, Langmuir 31 (2015) 3753-3762.

[21] Z. Luo, Y. Hu, K. Cai, X. Ding, Q. Zhang, M. Li, X. Ma, B. Zhang, Y. Zeng, P. Li, J. Li, J. Liu, Y. Zhao, Intracellular Redox-Activated Anticancer Drug Delivery by Functionalized Hollow Mesoporous Silica Nanoreservoirs with Tumor Specificity, Biomaterials 35 (2014) 7951-7962.

[22] X. Du, L. Xiong, S. Dai, F. Kleitz, S. Z. Qiao, Intracellular Micronevironment-Responsive Dendrimer-Like Mesoporous Nanohybrids for Traceable, Effective, and Safe Gene Delivery, Adv. Func. Mater. 24 (2014) 7627-7637.

[23] A. Raza, U. Hayat, T. Rasheed, M. Bilal, H. M. N. Iqbal, Redox-Responsive Nano-Carriers as Tumor-Targeted Drug Delivery Systems, Eur. J. Med. Chem. 157 (2018) 705-715.

[24] Y. Xiao, T. Wang, Y. Cao, X. Wang, Y. Zhang, Y. Liu, Q. Huo, Enzyme and Voltage Stimuli-Responsive Controlled Release System Based on β-Cyclodextrin-Capped Mesoporous Silica Nanoparticles, Dalton Trans. 44 (2015) 4355-4361.

[25] T. Wang, G. Sun, M. Wang, B. Zhou, J. Fu, Voltage/pH-Driven Mechanized Silica Nanoparticles for the Multimodal Controlled Release of Drugs, ACS Appl. Mater. Interfaces 7 (2015) 21295-21304.

[26] X. Jiao, R. Sun, Y. Cheng, F. Li, X. Du, Y. Wen, Y. Song, X. Zhang, A Voltage-Responsive Free-Blockage Controlled-Release System Based on Hydrophobicity Switching, ChemPhysChem 18 (2017) 1317-1323.

[27] N. M. Khashab, A. Trabolsi, Y. A. Lau, M. W. Ambrogio, D. C. Friedman, H. A. Khatib, J. I. Zink, J. F. Stoddart, Redox- and pH-Controlled Mechanized Nanoparticles, Eur. J. Org. Chem. (2009) 1669-1673.

[28] N. K. Guimard, N. Gomez, C. E. Schmidt, Conducting Polymers in Biomedical Engineering, Progress Polym. Sci. 32 (2007) 876-921.

[29] X. Wang, L. Zhi, K. Müllen, Conductive Graphene Electrodes for Dye-Sensitized Solar Cells, Nano Lett. 8 (2008) 323-327.

[30] S. J. Leigh, R. J. Bradley, C. P. Purssell, D. R. Billson, D. A. Hutchins, A Simple, Low-Cost Conductive Composite Material for 3D Printing of Electronic Sensors, PLoS ONE 7 (2012) e49365.

[31] D. Zhang, K. Ryu, X. Liu, E. Polikarpov, J. Ly,M. E. Tompson, C. Zhou, Transparent, Conductive, and Flexible Carbon Nanotube Films and Their Application in Organic Light-Emitting Diodes, Nano Lett. 6 (2006) 1880-1886.

[32] K. Liu, B. Liu, Recent Advances in Biodegradable Conducting Polymers and Their Biomedical Applications, Biomacromolecules 19 (2018) 1783-1803.

[33] H. Palza, A. P. Zapata, C. Angulo-Pineda, Electroactive Smart Polymers for Biomedical Applications, Materials 12 (2019) 277.

[34] M. Naseri, L. Fotouhi, A. Ehsani, Recent Progress in the Development of Conducting Polymer-Based Nanocompoites for Electrochemical Biosensors Applications: A Mini-Review, Chem. Rec. 18 (2018) 599-618.

[35] S. Inal, J. Rivnay, A.-O. Suiu, G. G. Malliaras, I. McCulloch, Conjugated Polymers in Bioelectronics, Acc. Chem. Res. 51 (2018) 1368-1376.

[36] Z. Aqrawe, J. Montgomery, J. Travas-Sejdic, D. Svirskis, Conducting Polymers as Electrode Coatings for Neuronal Multi-Electrode Arrays, Trends Biotechnol. 35 (2017) 93-95.

[37] H. Vara, J. E. Collazos-Castro, Biofunctionalized Conducting Poylmer/Carbon Microfiber Electrodes for Ultrasensitive Neural Recordings, ACS Appl. Mater. Interfaces 7 (2015) 27016-27026.

[38] R. Green, M. R. Abidian, Conducting Polymers for Neural Prosthetic and Neural Interface Applications, Adv. Mater. 27 (2015) 7620-7637.

[39] D. Svirskis, J. Travas-Sejdic, A. Rodgers, S. Garg, Electrochemically Controlled Drug Delivery Based on Intrinsically Conducting Polymers, J. Control. Release 146 (2010) 6-15.

[40] D. Uppalapati, B. J. Boyd, S. Garg, J. Travas-Sejdic, D. Svirskis, Conducting Polymers with Defined Micro- or Nanostructures for Drug Delivery, Biomaterials 111 (2016) 149-162.

[41] A. Alves-Sampaio, C. García-Rama, J.E. Collazos-Castro, Biofunctionalized PEDOT-Coated Microfibers for the Treatment of Spinal Cord Injury, Biomaterials 89 (2016) 98-113.

[42] B. Guo, P. X. Ma, Conducting Polymers for Tissue Engineering, Biomacromolecules 19 (2018) 1764-1782.

[43] R. Wadhwa, C. F. Lagenaur, X. T. Cui, Electrochemically Controlled Release of Dexamethasone from Conducting Polymer Polypyrrole Coated Electrode, J. Control. Release 110 (2006) 531-541.

[44] E. Shamaeli, N. Alizadeh, Nanostructured Biocompatible Thermal/Electrical Stimuli-Responsive Biopolymer-Doped Polypyrrole for Controlled Release of Chlorpromazine: Kinetics Studies, Int. J. Pharm. 472 (2014) 327-338.

[45] D. Esrafilzadeh, J. M. Razal, S. E. Moulton, E. M. Stewart, G. G. Wallace, Multifunctional Conducting Fibres with Electrically Controlled Release of Ciprofloxacin, J. Control. Release 169 (2013) 313-320.

[46] R. T. Richardson, A. K. Wise, B. C. Thompson, B. O. Flynn, P. J. Atkinson, N. J. Fretwell, J. B. Fallon, G. G. Wallace, R. K. Shepherd, G. M. Clark, S. J. O'Leary, Polypyrrole-Coated Electrodes for the Delivery of Charge and Neurotrophins to Cochlear Neurons, Biomaterials 30 (2009) 2614-2624.

[47] C. Boehler, N. Martini, Y. Xie, I. Dryg, T. Stieglitz, U.G. Hofmann, M. Asplund, Actively Controlled Release of Dexamethasone from Neural Microelectrodes in a Chronic *in vivo* Study, Biomaterials 129 (2017) 176-187.

[48] J. E. Collazos-Castro, J. L. Polo, G. R. Hernández-Labrado, V. Padial-Cañete, C. García-Rama, Bioelectrochemical Control of Neural Cell Development on Conducting Polymers, Biomaterials 31 (2010) 9244-9255.

[49] Y. Cho, R. Shi, A. Ivanisevic, R. Ben Borgens, Mesoporous Silica Nanosphere-Based Drug Delivery System Using an Electrically Conducting Polymer, Nanotechnology 20 (2009) 275102.

[50] A. García-Fernández, G. García-Laínez, M. L. Ferrándiz, E. Aznar, F. Sancenón, M. J. Alcaraz, J. R. Murguía, M. D. Marcos, R. Martínez-Máñez, A. M. Costero, M. Orzáez, Targeting Inflammasome by the Inhibition of Caspase-1 Activity Using Capped Mesoporous Silica Nanoparticles, J. Control. Release 248 (2017) 60-70.

[51] B. Lozano-Torres, L. Pascual, A. Bernardos, M. D. Marcos, J. O. Jeppesen, Y. Salinas, R. Martínez-Máñez, F. Sancenón, Pseudorotaxane Capped

Mesoporous Silica Nanoparticles for 3,4-Methylenedioxymethamphetamine (MDMA) Detection in Water, Chem. Commun. 53 (2017) 3559-3562.

[52] J. E. Collazos-Castro, G. R. Hernández-Labrado, J. L. Polo, C. García-Rama, N-Cadherin- and L1-Functionalised Conducting Polymers for Synergistic Stimulation and Guidance of Neural cell Growth, Biomaterials 34 (2013) 3603-3617.

[53] E. Garcia-Breijo, R. M. Peris, C. O. Pinatti, M. A. Fillol, J. I. Civera, R. B. Prats, Low-cost electronic tongue system and its application to explosive detection. IEEE Transactions on Instrumentation and Measurement 62(2) (2012) 424-431.

[54] N. K. Bhatti, M. S. Subhani, A. Y. Khan, R. Qureshi, A. Rahman, Heterogeneous Electron Transfer Rate Constants of Viologen Monocations at Platinum Disk Electrode, Turk. J. Chem. 30 (2006) 165-180.

[55] J. J. Orgill, C. Chen, C. R. Schirmer, J. L. Anderson, R. S. Lewis, Prediction of Methyl Viologen Redox States for Biological Applications, Biochem. Eng. J. 94 (2015) 15-21.

[56] L. Zhang, Progress in Molecular Biology and Translational Science, 93 (2010) 1–17.

[57] J. E. Collazos-Castro, C. García-Rama, A. Alves-Sampaio, Glial Progenitor Cell Migration Promotes CNS Axon Growth on Functionalized Electroconducting Microfibers, Acta Biomater. 35 (2016) 42-56.

[58] M. Ito, T. Kuwana, Spectroelectrochemical Study Of Indirect Reduction Of Triphosphopyridine Nucleotide: I. Methyl Viologen, Ferredoxin-TPN-Reductase and TPN, J. Electroanal. Chem. Interf. Electr. 32,3 (1971) 415-425.

[59] T. Nezakati, A. Seifalian, A. Tan, A. M. Seifalian, Conductive Polymers: Opportunities and Challenges in Biomedical Applications, Chem. Rev. 118 (2018) 6766-6843.

[60] F. Vitale, S. R. Summerson, B. Aazhang, C. Kemere, M. Pasquali, Neural Stimulation and Recording with Bidirectional, Soft Carbon Nanotube Fiber Microelectrodes, ACS Nano, 9 (2015) 4465-4474.

[61] Z. Cui, B. Yang, R-K. Li, Application of Biomateials in Cardiac Repair and Regeneration, 2 (2016) 141-148.

[62] B. Guo, X. Ma, Conducting Polymers for Tissue Engineering, Biomacromolecules, 19 (2011) 1764-1782.